Article

Current Biology

Circuit Mechanisms of a Retinal Ganglion Cell with Stimulus-Dependent Response Latency and Activation Beyond Its Dendrites

Highlights

- Unusual receptive field properties appear in a mouse retinal ganglion cell (RGC)
- Latency decreases with stimulus size and the RGC is activated beyond its dendrites
- Mechanisms of these phenomena involve inhibition and disinhibition
- This RGC may be involved in signaling image focus

Authors

Adam Mani, Gregory W. Schwartz

Correspondence

greg.schwartz@northwestern.edu

In Brief

Mani and Schwartz report the discovery of the "ON delayed" retinal ganglion cell (RGC) and describe its unusual receptive field properties. Synaptic mechanisms underlying this receptive field highlight new roles for inhibition and disinhibition in retinal circuits. The authors suggest a function for the ON delayed RGC in non-image-forming vision.

Mani & Schwartz, 2017, Current Biology *27*, 471–482
February 20, 2017
http://dx.doi.org/10.1016/j.cub.2016.12.033

CellPress

Current Biology
Article

Circuit Mechanisms of a Retinal Ganglion Cell with Stimulus-Dependent Response Latency and Activation Beyond Its Dendrites

Adam Mani[1] and Gregory W. Schwartz[1,2,3,4,*]
[1]Department of Ophthalmology, Feinberg School of Medicine, Northwestern University, Chicago, IL 60611, USA
[2]Department of Physiology, Feinberg School of Medicine, Northwestern University, Chicago, IL 60611, USA
[3]Department of Neurobiology, Weinberg College of Arts and Sciences, Northwestern University, Evanston, IL 60208, USA
[4]Lead Contact
*Correspondence: greg.schwartz@northwestern.edu
http://dx.doi.org/10.1016/j.cub.2016.12.033

SUMMARY

Center-surround antagonism has been used as the canonical model to describe receptive fields of retinal ganglion cells (RGCs) for decades. We describe a newly identified RGC type in the mouse, called the ON delayed (OND) RGC, with receptive field properties that deviate from center-surround organization. Responding with an unusually long latency to light stimulation, OND RGCs respond earlier as the visual stimulus increases in size. Furthermore, OND RGCs are excited by light falling far beyond their dendrites. We unravel details of the circuit mechanisms behind these phenomena, revealing new roles for inhibition in controlling both temporal and spatial receptive field properties. The non-canonical receptive field properties of the OND RGC—integration of long temporal and large spatial scales—suggest that unlike typical RGCs, it may encode a slowly varying, global property of the visual scene.

INTRODUCTION

Center-surround spatial organization is one of the core features of receptive field structure in visual neurons. Beginning at the first synapse in the retina, lateral inhibition shapes signals, creating antagonism between local (center) and global (surround) regions of visual space. Retinal ganglion cells (RGCs) were the first visual neurons to be described in terms of center-surround receptive fields [1], and the circuit mechanisms of receptive field structure have been studied extensively in the retina [2–4].

Alongside this classical view of receptive field structure has been a growing appreciation for the diversity of RGC types and their specific roles in detecting specific visual features [5–12]. Some of these feature detectors, such as object-motion-sensitive RGCs, rely on an antagonistic surround [7, 13], whereas others, such as M1 intrinsically photosensitive RGCs, eschew center-surround antagonism to suit their role in reporting global luminance [14]. Despite recent progress, few RGC types have been characterized in terms of unique electrophysiological responses, and circuit mechanisms responsible for such specific responses have only been identified for a handful of RGC types among the ~40 types thought to exist in the mammalian retina [12].

Here we describe a new type of RGC in the mouse, named the "ON delayed" (OND) RGC, whose receptive field structure deviates from the center-surround paradigm. Rather than being antagonized by large light stimuli, the OND RGC responds *earlier* than it does to smaller stimuli. The range of possible response latencies for OND RGCs is large, and the response to a stimulus of a size comparable to the cell's dendrites is unusually late. In addition, opposite to the usual antagonistic effect of the surround, firing in the OND RGC can be elicited by light patterns far outside its dendritic field. Our studies of the mechanisms responsible for these unusual receptive field characteristics yield new insights into the synaptic organization of retinal circuits and broaden our understanding of the varied roles of inhibition.

The canonical center-surround organization of RGCs serves to localize their spatial responses. The unusual characteristics of the receptive field of OND RGCs led us to suggest that they report a more global property of the scene, requiring integration rather than precisely reporting an event in time and space.

RESULTS

Functional and Morphological Classification of the ON Delayed RGC

As part of an effort to catalog the diversity of RGC light responses in the mouse, we encountered a set of cells with unusually long response latencies. Examples of ten of these OND RGCs responding to a 200 μm spot of light (intensity 100 rod isomerizations (R*)/rod/s, presented from darkness and centered on the receptive field) are shown in Figures 1A and 1B. Consistency of the response across trials (Figure 1C) suggested that the long latency was not a result of adaptation to repeated light flashes.

The response pattern was highly similar across cells within this group (Figure 1B), compared to ON RGCs outside this group that responded differently to the light step (Figure 1D). Whereas ON alpha, ON direction-selective, and ON orientation-selective are well-characterized RGC types (independently confirmed by

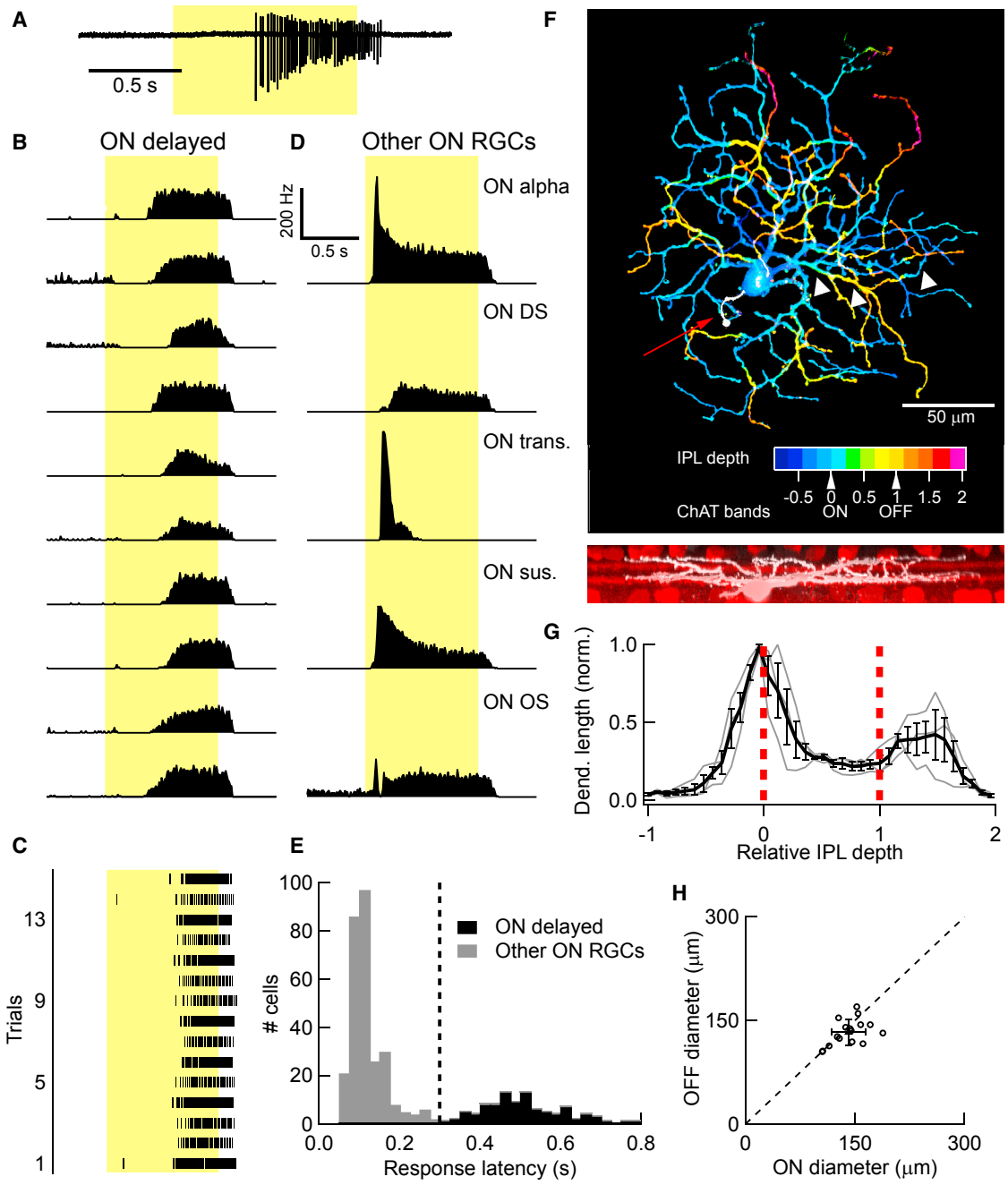

Figure 1. Light Response and Morphology of the OND RGC

(A) Light response of an OND RGC to a spot of light 200 μm in diameter, at 100 R*/rod/s presented from darkness ("Light Step"). Cell-attached spiking response in a single trial is shown. Duration of stimulus presentation is denoted by a yellow rectangle here and elsewhere.

(B) Peri-stimulus time histogram (PSTH) for ten representative OND RGCs responding to the light step stimulus, 10–20 trials each.

(C) Spike raster showing individual trials of an OND RGC responding to the light step.

(D) PSTH of spike activity in response to the light step stimulus in representative examples of five other RGC types computed from 10–20 trials each. ON DS, ON direction selective; ON OS, ON orientation selective; ON trans., ON transient; ON sus., ON sustained.

(E) Distribution of half-maximum latency in response to the light step across a sample of 382 RGCs containing ON non-direction-selective cells. Dashed line, classifier of OND cells at latency 0.3 s. Cells to the right of this line are OND cells (black), whereas cells to the left are not (gray).

(F) Top: maximum-projection confocal image of an OND RGC. The color scale represents depth within the inner plexiform layer (IPL). The red arrow points to an axon stub (white). White arrowheads point to a recursive dendrite. Arrows below the color scale denote IPL depth of the ON and OFF ChAT bands. Bottom: side view of the same cell, same scale (white), along with starburst amacrine cells and ChAT bands (red).

(legend continued on next page)

large somata, direction selectivity, and orientation selectivity, respectively), ON transient and ON sustained RGCs were grouped according to the temporal profile of their light responses and most likely each included multiple RGC types. The similarity in response profile among OND RGCs and their differences from other ON RGCs suggest that OND RGCs may consist of a single functional RGC type.

We further investigated the statistical separation of OND RGCs from other RGC types based on quantified properties of their light responses. OND RGCs were not direction selective when probed with moving bars (see the Experimental Procedures; direction selectivity index [DSI] = 0.05 ± 0.01, n = 14). ON direction-selective RGC cells also showed relatively long response latencies to a light step (0.28 ± 0.02 s, n = 54) but were easily distinguished from OND RGCs by their direction selectivity ($p < 10^{-10}$, unpaired t test; DSI = 0.39 ± 0.02, n = 56). Among non-direction-selective ON RGCs we recorded (DSI < 0.2), there was a significantly bimodal distribution of response latencies ($p < 10^{-5}$, Hartigan's dip test) with a clear separation at 0.3 s (Figure 1E). Thus, we established the threshold of 0.3 s latency to characterize ON non-direction-selective RGCs as OND.

A clear statistical separation of the OND RGCs from all other RGCs based on response latency provided evidence that OND RGCs may constitute a single RGC type. Results below show that cells classified by this functional criterion also shared characteristic receptive field properties not found in other RGCs, as well as other physiological and morphological characteristics, further supporting the claim that they represent a single RGC type. We found no evidence for heterogeneity within OND RGCs that would imply further splitting of this population into multiple types.

We filled and imaged OND RGCs to quantify their dendritic morphology (Figures 1F–1H; Figure S1). OND RGCs stratified near the ON choline acetyl-transferase (ChAT) band and distal to the OFF ChAT band (Figure 1G). This represents another example, along with the M1 intrinsically photosensitive (ip)RGC [15] and the ON orientation selective (OS) RGC [16], of a functionally pure ON RGC with an OFF dendritic stratification. We confirmed that OND RGCs retained pure ON polarity in photopic conditions (Figure S2).

OND RGCs had relatively small dendritic fields, with an equivalent diameter of 141 ± 23 μm (mean ± SD) in the ON stratum and 133 ± 19 μm (mean ± SD; n = 16) in the OFF stratum (Figure 1H). We also measured the longest axis through a polygon outlining the dendritic field in each stratum (Figure S1A). The long axes were only ~40% longer than the equivalent diameter, a sign of symmetric morphology shared by most RGCs [16–18]. We found OND RGCs in locations throughout the retina with no apparent gradient in density, function, or morphology.

The most distinctive morphological feature of OND RGCs was their recursive dendrites that extended to the OFF stratum before returning back to the ON stratum (Figure S1B). Recursive dendrites have been described in a different RGC type in rabbit and mouse, the suppressed-by-contrast RGC [19–22]. We found more and longer recursive dendrites in the OND RGC than in the mouse suppressed-by-contrast RGC or in two other bistratified RGC types (Figures S1C and S1D). The closest morphological match to the OND RGC in a public online database of electron-microscopic reconstructions is the "73" (http://museum.eyewire.org). More tentative matches exist in the published connectomics electron-microscopy data: gc31-56 from [23] and, in a recent functional study of RGC calcium signals, cluster no. 37, "ON slow" from [12]. We note that a morphologically similar cell to the OND RGC, the recursive bistratified RGC, has been found in non-human primates [24].

Inverted Size-Latency Tuning and Its Mechanism

To measure the extent and strength of the OND RGC receptive field center and surround, we presented light spots of varying sizes from darkness (to 100 R*/rod/s). Given the small dendritic field of the OND RGC, we expected to find a small receptive field center. Figure 2A shows the spike count during stimulus presentation normalized to its maximum as a function of spot size for OND RGCs and four other ON RGC groups. In fact, OND RGCs had surprisingly large receptive fields (maximal response diameter, 386 ± 30 μm, n = 16) given their dendritic diameter. Unlike most RGC types [7, 16, 25] (Figure 2A), OND RGCs showed very little surround suppression.

An unusual feature of the OND RGC's response to the spot stimuli was its inverted size-latency tuning (Figure 2B). Whereas other RGCs either increased response latency or showed no change in latency with increases in spot size, OND RGCs responded *earlier* to larger spots. The range over which the latency varied with spot diameter was large (0.3 ± 0.02 s, n = 20) compared to that observed in RGCs in the mouse and other species [26]. Examples for the same cell responding at five spot sizes are shown in Figure 2C, together with examples of two other RGCs for comparison. We also measured inverted size-latency tuning in OND RGCs in photopic conditions indicating that this feature of the response was robust across luminance conditions (Figure S3).

To determine the mechanisms responsible for inverted size-latency tuning, we performed whole-cell voltage-clamp recordings from OND RGCs (Figure 3). Excitation to the OND RGC (peak current, −122 ± 10 pA, n = 11) occurred only at light onset, was slow and sustained, and sometimes had a small very transient initial component (Figure 3B). Inhibition was large compared to excitation (peak current, 750 ± 70 pA, n = 13; maximum excitation-to-inhibition ratio of peak current across cells, 0.2 ± 0.02, n = 11), present at light onset and offset, and more transient than excitation. Two features of the synaptic conductances were distinct from patterns typically observed in RGCs. First, inhibition had stronger surround suppression than excitation (Figure 3A). Second, inhibition had a shorter latency (Figure 3C) and shorter duration (Figure 3D) than excitation. The duration of the inhibitory conductance also showed a

(G) Dendritic density profile. IPL depth is in normalized coordinates, where 0 and 1 correspond to the ON and OFF ChAT bands, respectively (red dashed lines). Gray lines, individual cells; black, mean density ± SEM (n = 3 cells).

(H) Equivalent diameter of the dendritic fields of the ON and OFF strata of OND RGCs (see the Experimental Procedures). Empty circles, OND cells; filled symbol and error bars, mean ± SD (n = 16 cells). The dashed line is the line of equal ON and OFF dendritic diameters.

See also Figures S1 and S2.

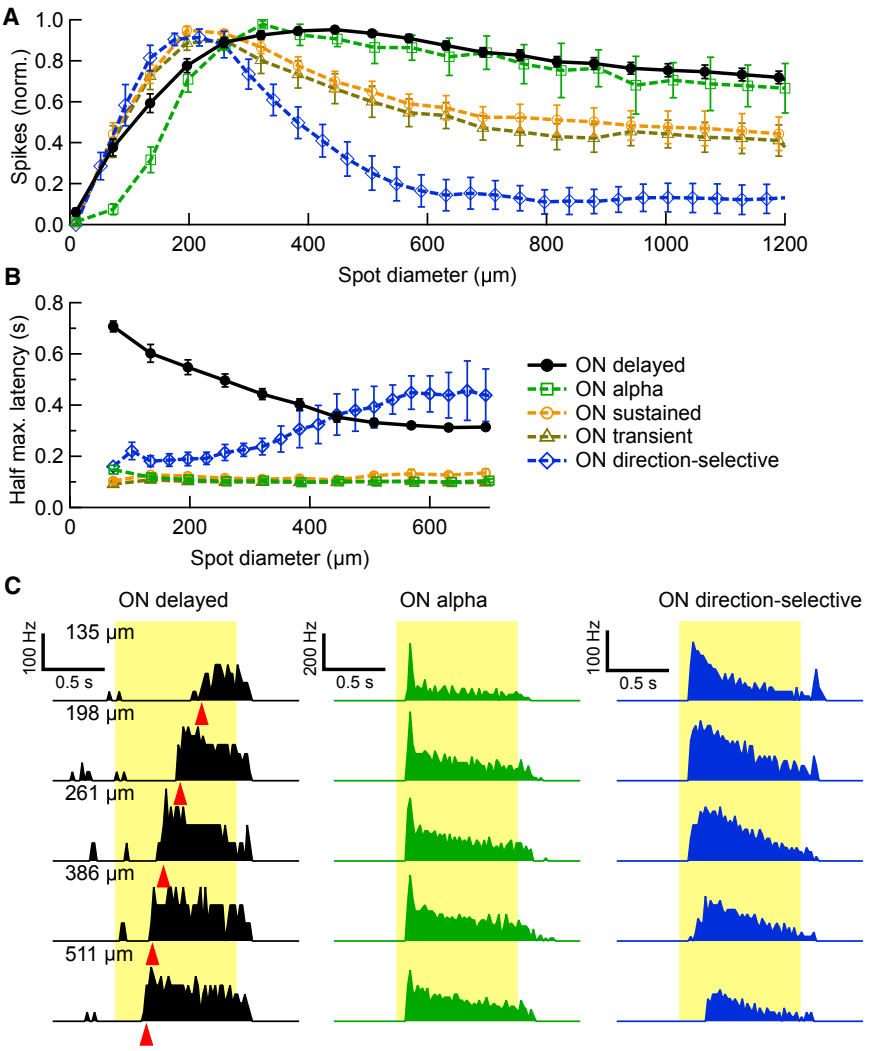

Figure 2. Response Latency and Spike Count as a Function of Stimulus Size

(A) Spike count during stimulus presentation versus spot diameter, normalized by its maximum (average ± SEM over cells within each group). Numbers of cells: OND, n = 16; ON alpha, n = 4; ON direction-selective, n = 6; ON sustained, n = 13; ON transient, n = 9.

(B) Half-maximum latency versus spot diameter (average ± SEM over cells within each group).

(C) PSTH of an OND RGC (black), ON alpha RGC (green), and ON direction-selective RGC (blue) in response to spots of different sizes. Spot sizes are denoted at the upper left of each row. From PSTHs, spike count and latency were extracted. Red triangles, half-maximum latency for the OND PSTHs.

See also Figure S3.

marked dependence on spot size, becoming briefer for larger spots (Figure 3D).

These distinct patterns of excitation and inhibition make a prediction about the mechanism of inverted size-latency tuning in the OND RGC. Although steady excitation is required to depolarize the cell, rather than firing near the onset of excitation, OND RGC firing is initiated by a release from inhibition. The latency of this release from inhibition decreases with increasing spot size because inhibition becomes smaller and more transient, whereas excitation remains sustained and has less suppression. To test whether the synaptic conductances were sufficient to explain inverted size-latency tuning, we created a leaky integrate-and-fire model of the spiking activity of OND RGCs (Figures 3E–3I). Converting measured synaptic currents into conductances (Figure 3E) and feeding them into the model, we simulated membrane voltage dynamics in response to spots of varying sizes (Figure 3F). The only parameters that were chosen per cell were the spiking threshold and an increased time constant following a spike. Fixing these based on the spiking response measured for the same cell at a single spot size (200 μm), we then produced simulated data across the range of spot sizes (Figures 3G–3I). The model captured the general shape of the OND RGC's light response (Figure 3G) and inverted size-latency tuning (Figure 3H). Surround suppression (Figure 3I) seemed somewhat stronger than in experimental results. This may be due to an additional current we discovered arising from stimuli beyond the RGC dendrites (see Figures 5 and 6). This current was not included in the model directly, with its own driving force, but only via its contribution to the measured excitatory (cation) and inhibitory (chloride) currents.

Pharmacology of Synaptic Inputs to the OND RGC

To gain insights into the circuitry upstream of the OND RGC, we repeated our whole-cell receptive field measurements in the presence of different inhibitory receptor blockers. Our pharmacology experiments included gabazine, TPMPA ((1,2,5,6-Tetrahydropyridin-4-yl)methylphosphinic acid), and/or strychnine to block γ-aminobutyric acid receptor type A ($GABA_A$), $GABA_C$, or glycine receptors, respectively (Figure 4). Two main results came from this set of experiments. First, light-induced inhibitory currents are completely dependent on a combination of glycine and $GABA_A$ receptors. Blocking both of these receptor types with gabazine + strychnine eliminated inhibitory currents completely (Figures 4A and 4C). The effects of the two blockers were not additive, however. Gabazine alone did not substantially reduce the total charge of inhibitory currents in OND RGCs, and strychnine alone reduced the currents to about 40% of their control charge. Non-additivity of these blockers suggests an upstream interaction between GABAergic and glycinergic circuits (see model below).

Second, the strong surround suppression of the inhibitory currents that we found to be critical for inverted size-latency tuning (Figure 3) relies on a combination of $GABA_A$ and $GABA_C$ receptors. Both the total charge (Figures 4A and 4C) and the duration (Figures 4B and 4C) of inhibition were increased in the presence

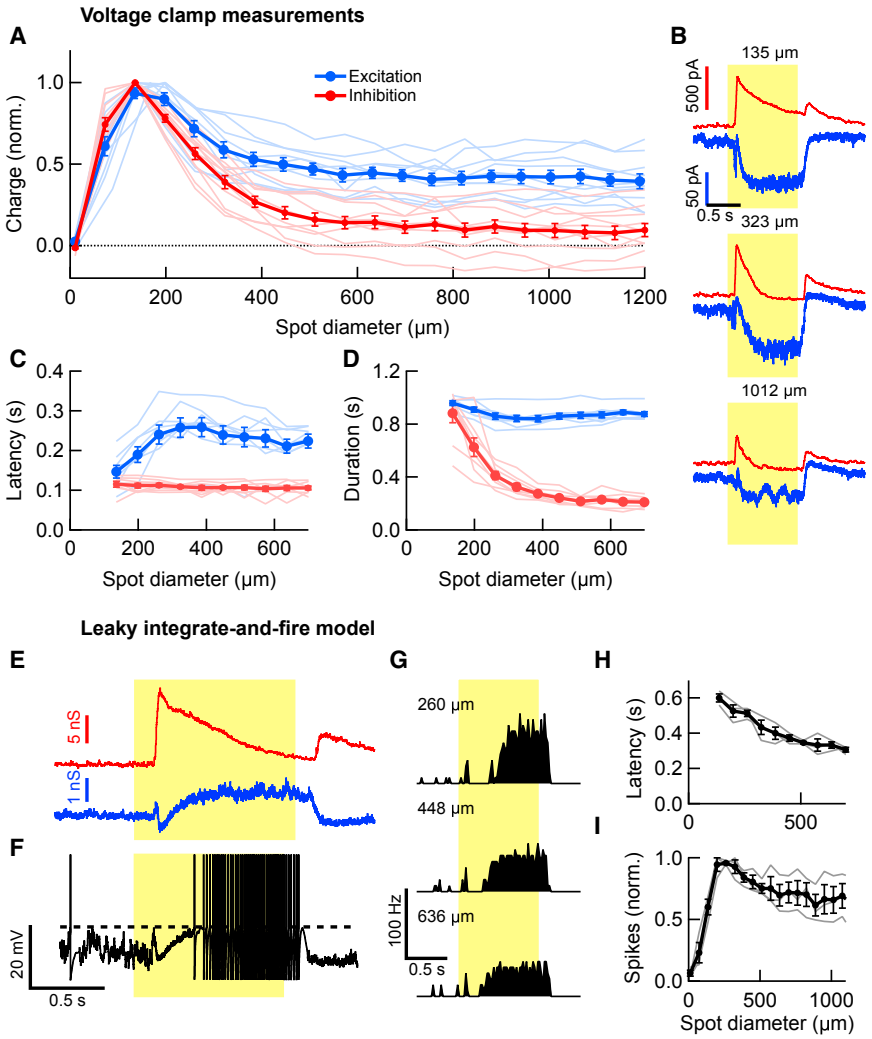

Figure 3. Stimulus Size Dependence of Synaptic Currents in OND RGCs and the Leaky Integrate-and-Fire Model

(A) Total charge of excitatory (blue, n = 10 cells) and inhibitory (red, n = 11 cells) currents in OND RGCs, normalized by their maximum, as a function of spot diameter. Thin lines, individual cells; thick lines, mean ± SEM throughout the figure.

(B) Excitatory and inhibitory currents as a function of time, measured in an OND RGC for three different spot sizes, denoted above each panel (mean traces over three trials, with the same colors as in the main figure). From current time traces, charge, latency, and duration were extracted.

(C) Latency of excitatory (blue) and inhibitory (red) response currents as a function of spot diameter. Inhibition was earlier than excitation: spot diameter $\geq$ 197 μm; $p < 0.0013$, one-tailed paired t test (n = 8 cells).

(D) Duration of excitatory (blue) and inhibitory (red) response as a function of spot diameter. Inhibition was more transient than excitation: spot diameter $\geq$ 197 μm; $p < 0.0017$, one-tailed paired t test (n = 8 cells).

(E) Excitatory (blue) and inhibitory (red) synaptic conductances in an OND RGC in response to a 200 μm diameter spot, obtained directly from measured synaptic currents (such as those in B), and fed into the leaky integrate-and-fire model.

(F) Resulting simulated membrane potential, using conductances in (E). The dashed line is the spiking threshold.

(G) Simulated PSTH for different spot diameters that are denoted on the left. Each PSTH was calculated from the spiking in 12 simulated trials.

(H) Simulation half-maximum latency versus spot diameter for three different OND cells (thin lines); thick line, average curve ± SEM.

(I) Spike counts versus spot diameter, for the same cells and simulated data as in (H). Thin lines, individual cells; thick line, average ± SEM (n = 3 cells).

of TPMPA and increased more in the presence of TPMPA + gabazine. Again, the effects of TPMPA and gabazine were non-additive, suggesting an upstream interaction. Our results are consistent with the simplified model of the inhibitory circuit upstream of OND RGCs shown in Figure 4D. In this model, narrow-field glycinergic and GABAergic amacrine cells provide inhibition onto the dendrites of the OND RGC. Wide-field GABAergic amacrine cells in turn inhibit the narrow-field amacrine cells via $GABA_A$ and $GABA_C$ receptors. Although the diagram in Figure 4D is the simplest circuit consistent with our data, other interactions are possible. The amacrine cells shown are not necessarily single types, and they may interact with each other either directly or through the bipolar cells providing excitatory input to them.

Similar experiments measuring the pharmacology of excitatory currents with the same set of inhibitory receptor blockers yielded two main results (Figure S4). First, surround suppression of excitatory currents is predominantly provided by GABAergic inhibition onto $GABA_C$ receptors, presumably located on bipolar cell terminals. We also observed an apparent strengthening of the surround of excitatory currents when blocking either $GABA_A$ receptors alone or $GABA_A$ and glycine receptors. Later experiments suggested that the reduction of current by these blockers was at least in part due to a source other than glutamate from bipolar cells (see Figures 5 and 6). Second, we found that presynaptic inhibition shapes the kinetics of the excitatory currents, contributing to their slow rise by eliminating an early transient component. This inhibition is provided by $GABA_A$ and glycine receptors. In summary, interactions between $GABA_A$, $GABA_C$, and glycine inhibition shape the spatial and temporal properties of the excitatory and inhibitory currents onto OND RGCs, leading to the unusual properties of the currents and, ultimately, to inverted size-latency tuning in the spike responses of the RGC.

The OND RGC Can Be Stimulated by Light Falling Outside Its Dendrites

Surround suppression of spiking responses was weak for the OND RGC; only ON alpha RGCs had a similarly weak surround among the ON RGCs we tested (Figure 2A). Weak surround suppression could merely be the result of weak inhibition onto both the RGC and its presynaptic bipolar cells for large spots.

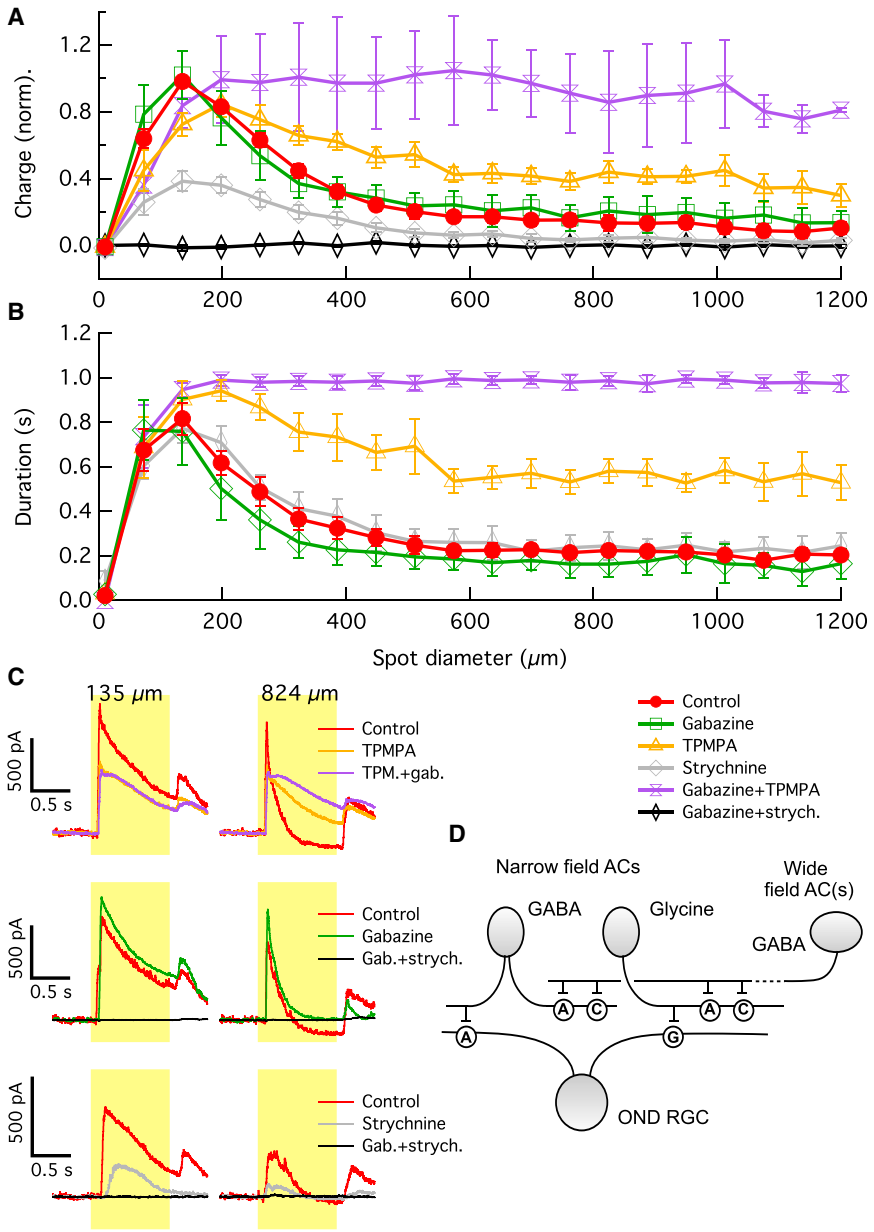

Figure 4. Stimulus Size Dependence of Synaptic Inhibitory Currents of OND RGCs in the Presence of Synaptic Blockers

(A) Charge of the inhibitory current in OND RGCs versus spot diameter in the control condition (red, n = 8 cells), in the presence of gabazine blocking $GABA_A$ receptors (green, n = 4 cells), TPMPA blocking $GABA_C$ receptors (orange, n = 4 cells), strychnine blocking glycine receptors (gray, n = 3 cells), TPMPA + gabazine (purple, n = 3 cells), and strychnine + gabazine (black, n = 4 cells). Curves, mean ± SEM over cells.

(B) Duration of inhibitory current in OND RGCs versus spot diameter, measured as the time the current was >25% of its maximum value (see the Experimental Procedures). Colors of curves are as in (A). Curves, mean ± SEM over cells.

(C) Traces of inhibitory current versus time in OND cells, measured for two different spot sizes denoted above. Colors of traces are as in (A). Each trace is an average over three trials.

(D) Diagram of the circuit model to explain the results in (A)–(C). AC, amacrine cell; neurotransmitters produced by ACs appear next to somas. A, C, and G are synapses containing $GABA_A$, $GABA_c$, and glycine receptors, respectively.

See also Figure S4.

However, the discrepancy between the small dendritic field of OND RGCs and the observed size of the receptive field center (Figure 2A) motivated us to further test the response of OND RGCs to light stimuli beyond the RGC dendrites.

To test for activation by distant stimuli, we presented annuli of fixed width and varying diameters while measuring the spike responses of both OND RGCs and ON alpha RGCs (Figure 5A). The response curves were compared with the dendritic diameter for each of the cell types (Figure 5A, vertical bars). Whereas ON alpha RGC responses declined sharply for annuli outside the dendritic field, OND RGCs responded to stimuli far outside their dendrites. Spikes elicited by annuli outside the dendritic field were apparent in the OND RGC but not the ON alpha (Figure 5A). Despite the fact that ON alpha RGCs fire twice as many spikes as OND RGCs at their receptive field maxima, a 480 μm inner diameter annulus elicited 20 ± 2 spikes in OND RGCs (n = 20) and 7 ± 3 spikes in ON alpha RGCs (n = 6). Thus, the seemingly similar weak surround suppression observed for both the ON alpha RGC and the OND RGC using spots (Figure 2A) may be due, in part, to different mechanisms, as revealed by the annulus stimulus. ON alpha RGCs have weak suppression but no activation beyond their dendrites, whereas OND RGCs receive extra-dendritic activation.

Extra-Dendritic Activation via Disinhibition

What synaptic mechanism accounts for extra-dendritic responses in the OND RGC? Many studies have shown excitation in RGCs to be coextensive with their dendrites [27–29]. This is an intuitive result because the receptive fields of bipolar cells, which provide excitation to RGCs, are typically much smaller (~45 μm) [30, 31] than those of RGCs (~250 μm) [12]. Again we turned to voltage-clamp measurements to determine the source of the extra-dendritic activation, clamping the membrane voltage at either 11.4 mV (near the non-specific cation reversal potential) or −68.6 mV (near the chloride reversal potential), in an attempt to isolate inhibitory and excitatory currents, respectively (Figure 5B). Consistent with the decreased inhibition for large spots (Figure 3A), annuli beyond the dendritic field of the OND RGC elicited no outward inhibitory currents but, surprisingly, we measured inward currents at both the chloride and non-specific cation reversal potentials in response to annuli well outside the RGC

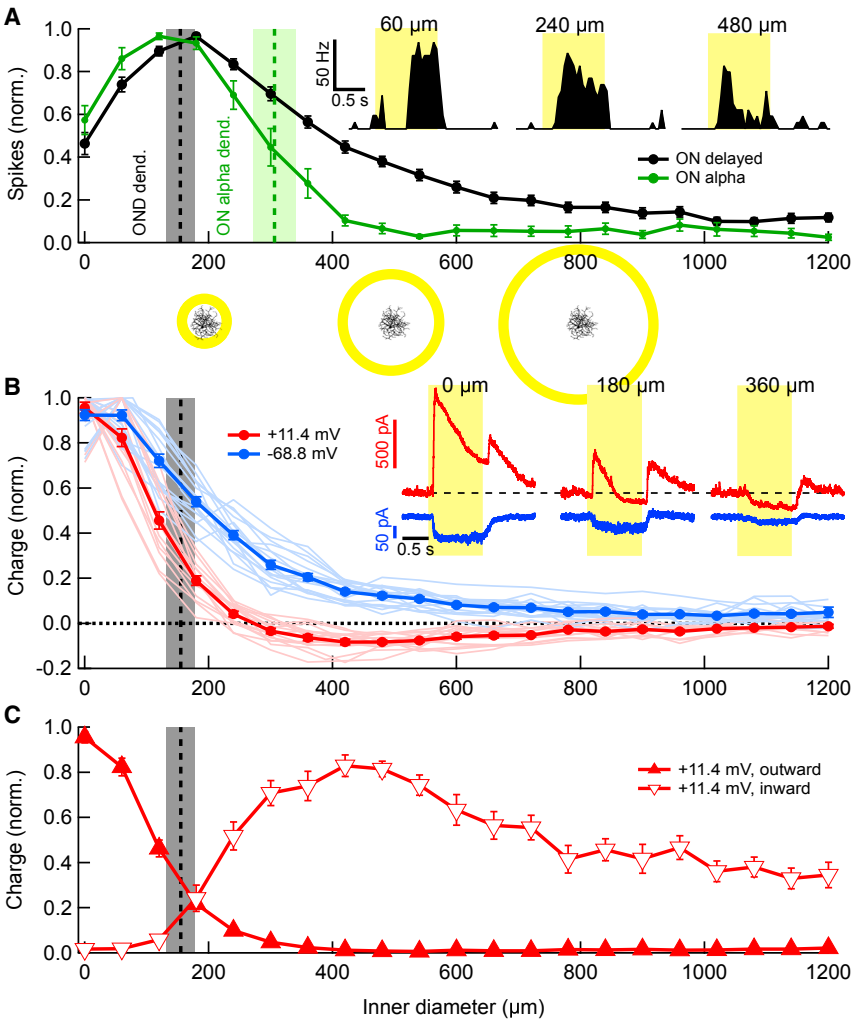

Figure 5. Responses of OND to Light Annuli with Varying Diameters

(A) Spike count during stimulus presentation (normalized by maximum) versus inner diameter of a bright annulus of constant 60 µm width, shown for OND (black, n = 20 cells) and ON alpha RGCs (green, n = 6). Curves, mean over cells ± SEM throughout the figure. Maximum absolute numbers of spikes were 49 ± 2 and 98 ± 11 in OND and ON alpha RGCs, respectively. Vertical bars in (A) and (B) are dendritic diameters of OND and ON alpha (mean ± SD; OND cells, n = 18; ON alpha cells, n = 3). Stimulus schematics along with an OND cell are shown to scale below corresponding values on the horizontal axis. Inset: PSTH in an OND RGC for three different annulus inner diameters, denoted above.

(B) Total charge of synaptic currents in OND RGCs versus inner diameter of annuli, measured at a holding voltage of −68.6 mV (blue) and +11.4 mV (red) and normalized by their maximum (−68.6 mV, 18 cells; +11.4 mV, 15 cells). Inset: currents versus time at holding voltages of −68.6 and +11.4 mV in an OND RGC for three different annulus inner diameters, denoted above (mean traces over three trials; colors are as in the main panel).

(C) Charge calculated and normalized separately for the outward (closed symbols) and inward (open symbols) components of the currents at a holding voltage of +11.4 mV.

dendrites (Figures 5B and 5C). This suggested that perhaps a circuit distinct from those active within the dendritic field of the OND RGC provides activation beyond the dendritic field.

To explore the identity of these currents further, we recorded light responses from OND RGCs for both a spot and an annulus while holding the membrane potential at a range of values (Figure 6). Using a small spot and a large annulus allowed us to measure the current-voltage relationships of the synaptic conductances elicited by light stimuli either within or outside the dendritic field of the RGC. A 200 µm diameter spot, covering mostly the area of the dendrites, elicited a response family as seen in Figure 6A. Consistent with the currents recorded at only two different potentials (Figure 5B), the early part of the response (at 200 ms) was dominated by an inhibitory chloride current (reversing at −55.8 ± 2 mV, n = 7; Figure 6C), whereas the late part of the response included a substantial excitatory component and thus had a reversal potential between the chloride and non-specific cation reversal potentials (−22.7 ± 5 mV, n = 6; Figure 6C).

The light response elicited by annuli (400 µm inner diameter) outside the dendritic field had only a late, sustained component (Figure 6B), and this current had a very different voltage dependence from those elicited by the spot (Figure 6C). Surprisingly, this current became more negative (inward) with increasing holding voltage, and had an apparent reversal at −72.8 ± 2 mV (n = 7). The fact that the size of this current depended on the holding potential excludes gap junctions as its source, as gap-junctional currents are characterized by flat current-voltage relationships. The "inverted" current-voltage relationship could be explained by disinhibition, the removal of a tonic inhibitory conductance by stimuli outside the RGC dendrites. However, the current reversed at a potential too negative for it to be carried by chloride. Therefore, we hypothesized that the tonic inhibition removed by extra-dendritic stimuli may at least in part be carried by a potassium conductance, which would account for its negatively shifted reversal potential. This would be the case if potassium channels controlled by metabotropic $GABA_B$ receptors mediate this current. Whereas voltage-gated potassium channels were blocked in our recordings by cesium ions present in the recording pipette, the inward-rectifying potassium channels associated with $GABA_B$ receptors are unaffected by internal cesium block [32].

Again we turned to pharmacology experiments to reveal the circuit elements leading to this extra-dendritic disinhibition. Whereas TPMPA (a $GABA_C$-receptor antagonist) had no effect on the disinhibitory current, gabazine (a $GABA_A$-receptor antagonist) eliminated it completely (Figure S5). Tetrodotoxin also had no effect on the disinhibitory current (data not shown), suggesting that neither spiking amacrine cells nor sodium channels in other cells in the retina participate in this circuit. Whereas

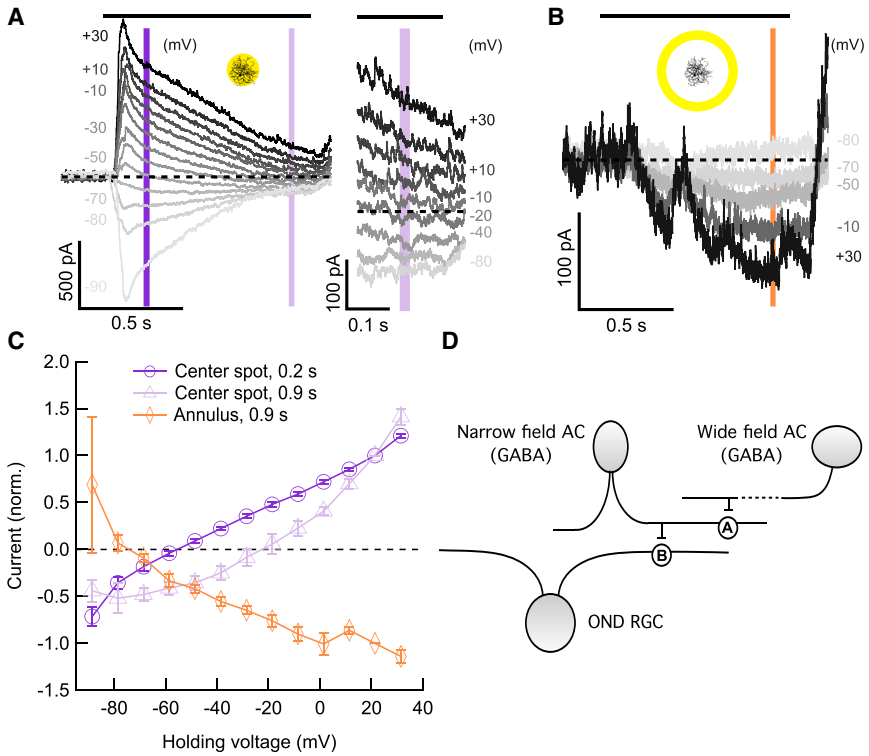

Figure 6. Current-Voltage Relationships in Response to a Spot and Annulus

(A) Left: currents versus time at different holding voltages in an OND RGC, in response to a center spot of light (200 μm, 200 R*/rod/s from darkness). Right: same currents as in the left panel, zoomed in on the last 0.2 s of the presentation of the spot. Curves for some voltages were omitted for clarity. Horizontal black bars, time of stimulus presentation. Dashed lines, zero current. Vertical purple bars denote time points used in (C). Insets show light stimulus schematics.

(B) Currents versus time at different holding voltages in an OND RGC in response to a light annulus (400 μm inner diameter, 520 μm outer diameter, 200 R*/rod/s from darkness, n = 7 cells). Vertical orange bar, time point used in (C). Insets show light stimulus schematics.

(C) Current versus holding voltage curves (mean ± SEM, n = 7 cells) at time points 0.2 s (dark purple) and 0.9 s (light purple) in response to a center spot of light as in (A), as well as a similar curve taken at time point 0.9 s, in response to a light annulus as in (B).

(D) Diagram of the model for circuitry to explain the extra-dendritic current (B and C) and elimination of it by blocking $GABA_A$ and $GABA_B$ receptors (Figure S5). See the main text. AC, amacrine cell; A, synapse containing $GABA_A$ receptors; B, synapse containing $GABA_B$ receptors, providing tonic inhibition onto the OND RGC.

See also Figure S5.

the extra-dendritic disinhibitory current was eliminated by gabazine, the inhibitory chloride current elicited by stimuli within the dendritic field of the RGC was unchanged in amplitude (Figure S5A). Consistent with the hypothesis that metabotropic activation of a potassium current was involved in the extra-dendritic current, the $GABA_B$-receptor agonist baclofen eliminated the extra-dendritic current while leaving (chloride-mediated) inhibition within the dendritic field intact (Figure S5).

The diagram in Figure 6D summarizes our conclusions regarding the extra-dendritic current. OND RGCs may receive a tonic inhibitory conductance from a GABAergic amacrine cell, via $GABA_B$ receptors. The amacrine cell is in turn inhibited, via $GABA_A$ receptors, by a wide-field (non-spiking) GABAergic amacrine cell that is activated by distant light stimulation. In summary, extra-dendritic activation in the OND RGC (Figure 5A), which contributes to its receptive field center being larger than its dendritic field and its weak surround suppression (Figure 2A), may rely on release from tonic inhibition via a serial inhibitory circuit.

DISCUSSION

An RGC Type with Unusual Receptive Field Characteristics

The long history of research on the light responses of RGCs spanning over seven decades and numerous species has uncovered many different types of receptive fields. To our knowledge, the OND RGC represents a receptive field structure that has not been reported in any of the previous literature. Two of its key functional attributes, inverted size-latency tuning and extra-dendritic activation, are unique among reported RGC receptive fields and among those we have measured. The unusual firing pattern of the OND RGC—in particular its long delay (Figure 1)—provides a reliable measure for functional targeting in wild-type mice, which can easily be further verified by testing for inverted size-latency tuning (Figure 2B). This targeting scheme should enable the OND RGC to be studied systematically across multiple labs.

New Functional Roles for Inhibition in Retinal Circuits

Two aspects of the role of inhibition in the non-canonical circuitry of the OND RGC are of general importance in sensory and systems neuroscience. The timing of the currents causes the RGC to spike upon release from inhibition, controlling the cell's unusual response-latency pattern (Figures 2 and 3). A combination of distinct inhibitory pathways gives rise to these special characteristics in the synaptic inputs (Figure 4; Figure S4). The ON direction-selective RGC in rabbit has a similar release from inhibition mechanism to control speed dependence [33]. Glycinergic inhibition has also been shown to play a key role in delaying the onset of spiking in rabbit local edge detector RGCs [34].

Second, we show a role for disinhibition in activating the RGC with stimuli far beyond its dendritic field (Figures 5 and 6). Disinhibition of a tonic glycinergic current onto the RGC is known to play an important role in the responses of the two OFF alpha RGC types [5, 35]. Disinhibition in the OND RGC does not reverse at the reversal potential for chloride (Figure 6C) and instead is most likely carried by a tonic $GABA_B$-receptor-mediated potassium conductance (Figure S5). Unlike the disinhibitory currents measured in OFF alpha cells, the current we measured

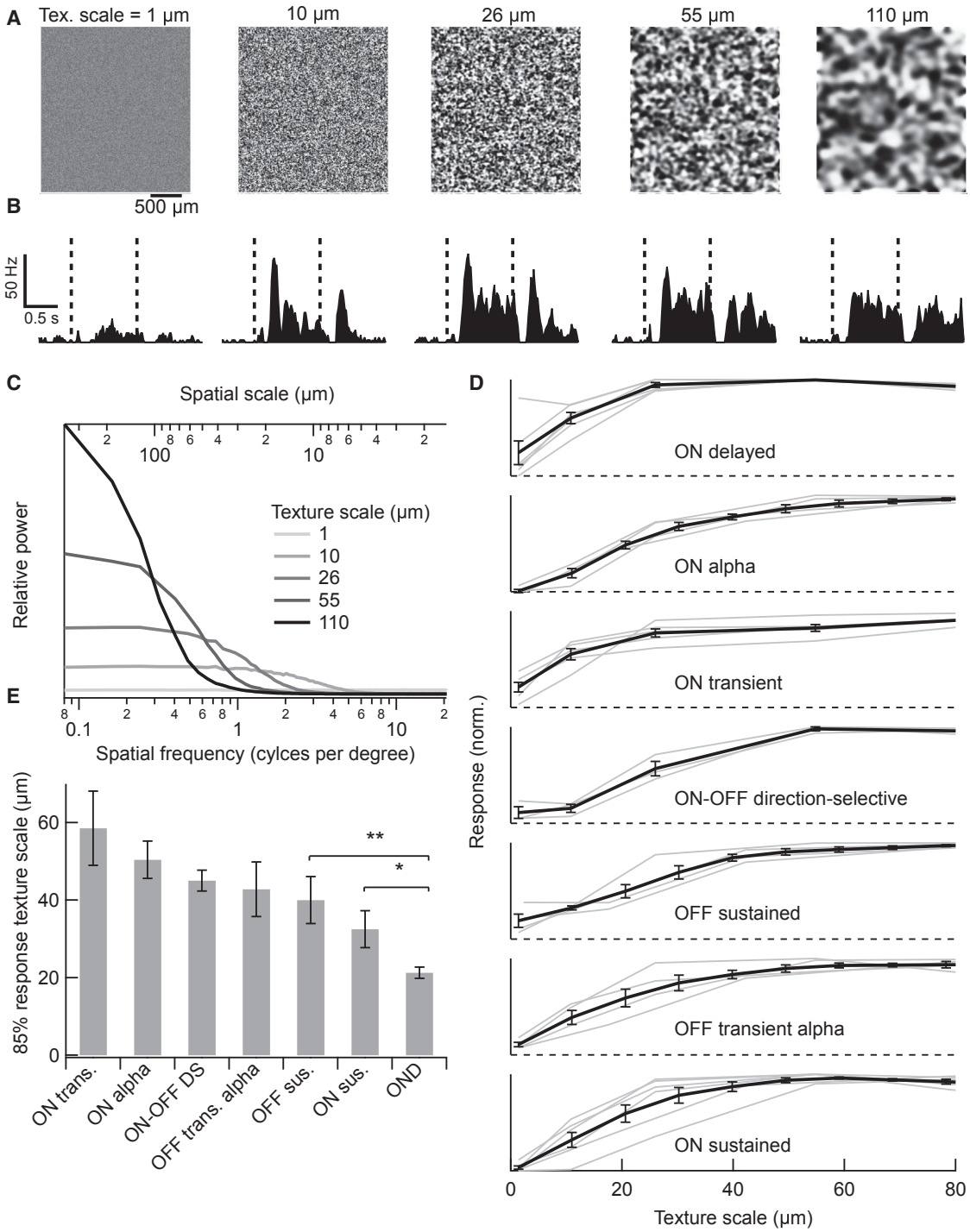

Figure 7. Response of OND RGCs to Random Textures with Varying Degrees of Blur

(A) Full-field textures, made with the same random seed and varying Gaussian blur. Denoted above each texture is the cutoff spatial scale ("texture scale"; see the main text and Experimental Procedures).

(B) PSTHs measured in an OND RGC in response to each corresponding spatial scale as in (A). Each PSTH was taken over 15–20 trials in response to different images having the same spatial scale. A texture was presented during the time between the dashed lines, and a uniform background having the same mean luminance (1,000 R*/rod/s) was presented before and afterward.

(C) Spatial frequency content in textures. Relative power versus spatial frequency (bottom horizontal axis) or spatial scale = (spatial frequency)$^{-1}$ (top axis). Curves are empirically measured averages over 500 texture patterns at each blur size.

(legend continued on next page)

was selectively activated for stimuli beyond the dendrites of the RGC (Figures 5 and 6).

Our pharmacology results (Figure 4; Figures S4 and S5) constrain models of the circuits upstream of the OND RGC that shape the excitatory, inhibitory, and disinhibitory currents we measured in the RGC. Generally, these results support previous studies of the different receptors mediating direct inhibition onto RGCs, serial inhibition between amacrine cells, and surround inhibition onto bipolar cell terminals [34, 36, 37]. In particular, our results support the role of $GABA_C$ receptors in lateral inhibition in retinal interneurons (onto both amacrine and bipolar cells), but not directly onto RGCs. $GABA_C$ receptors limit the spatial extent of inhibitory currents into the OND RGC and control their decay in time. We found multiple roles for $GABA_A$ and glycine receptors in the OND RGC circuit, consistent with previous reports of their function in other retinal circuits [38]. Our finding that $GABA_B$ receptors provide tonic inhibition that is suppressed by extra-dendritic activation in OND RGCs represents a new role for $GABA_B$ receptors in a retinal circuit.

A Large Dynamic-Range Latency Code

RGC response latency can depend on a variety of features of the visual stimulus, and spike-latency codes have been implicated in encoding contrast and spatial structure [26, 39, 40]. Latency shifts at steady luminance due to parameters such as contrast, which has been linked to temporal coding, are on the order of several tens of milliseconds [26, 40]. Remarkably, the OND RGC response-latency shifts by more than 300 ms with spot size (Figure 3B).

Whereas the kinetics of many parts of retinal circuits, including phototransduction, accelerate with increasing luminance, the long latency of response of OND RGCs and the stimulus size-latency tuning are robust to a change in luminance (Figure S3). The OND RGC may thus encode spatial information temporally. The role of the latency shift in the encoding strategy of the OND RGC remains unclear, and future studies with a wide range of stimuli may uncover how multiple stimulus features interact to control response latency.

A Possible Role for the OND RGC in Encoding Global Image Focus

What could be the function of the OND RGC? A canonical center-surround organization decorrelates responses of neighboring RGCs and enables them to report properties of the visual scene locally (i.e., occurring only in the receptive field center) [41]. An exception is the M1 ipRGC, which exhibits no surround suppression [14] and encodes global luminance [42], rather than local information. RGCs usually also respond quickly, with latencies comparable to the minimal time delay imposed by phototransduction.

By contrast, OND RGCs respond to rather large stimuli and respond slowly. We suggest that spatial localization and speed are traded off in the OND RGC for achieving high sensitivity, via integration over time and space, in detecting a property of the visual field that is not highly localized and varies slowly. We further speculate that this property may be the degree of image focus detected by the retina.

Defocusing an image changes its spatial frequency content, attenuating high frequencies [43]. We measured RGC responses to full-field spatial patterns with equal distributions of positive and negative contrasts but varying degrees of blur and hence varying spatial frequency content [31] (Figures 7A and 7C; see the Experimental Procedures). The mean intensity in each texture was equal to that of the background presented before and after it (1,000 R*/rod/s). OND RGCs fired at either the onset or offset of texture patterns, or at both times (Figure 7B). Note that the presence of texture onset and offset responses does not imply a light OFF response because there was no net change in overall light intensity between texture and background. Because we were interested in the dependence of RGC responses on spatial blur and not on local variations in contrast across textures, we quantified the response by summing spikes at onset and offset and averaging across five different texture patterns at each spatial scale. Among RGCs we measured, only some cell types, including OND RGCs, responded well to the texture stimulus (>10 Hz; Figure 7D), whereas the rest responded poorly or not at all (38 of 70 cells). Moreover, OND RGCs were sensitive to the highest spatial frequencies; the texture scale at which the OND RGC reached 85% of its maximal response (21.3 ± 1.4 μm, n = 6) was the smallest among RGC types we measured (Figure 7E). Thus, the OND RGC is exquisitely sensitive to local contrast in a full-field image. The limiting frequency is consistent with both the resolution of single bipolar cells [30, 31] and the spatial frequency limit of mouse vision [44].

The OND RGC's sensitivity to fine spatial scales is consistent with a model of nonlinear subunits for the receptive field of an ON RGC, with the onset-to-offset response ratio depending on the alignment of the bright and dark patches of the texture with receptive field subunits [31]. Mechanistic connections between this texture sensitivity and the other receptive field properties described in the Results remain to be explored in future experiments and modeling. The firing of OND RGCs is not selective solely for fine textures, and this one RGC type alone probably does not carry the full representation of image focus. Nonetheless, we think that it is a good candidate for a role within the focus detection circuit, given the above considerations.

Although its cellular substrate is yet to be discovered [45], an image focus signal exists within the retina. During development, this signal controls emmetropization, the process matching the dimensions of the eye with its refractive power, in species including mouse and human [46, 47]. Normal emmetropization depends on the ON pathway of the retina [48]; disruption of this process results in disorders of refractive index, such as myopia. A signal of image focus may also have use in the adult animal, in visual accommodation, which brings the retinal image into focus. Although the well-known lens accommodation

(D) Spike count during both stimulus onset and offset versus texture scale, normalized by its maximum. Thin curves, individual cells; thick curves, average ± SEM over cells within each group. Numbers of cells: OND, n = 6; ON alpha, n = 4; ON transient, n = 5; ON-OFF direction selective, n = 3; OFF sustained, n = 4; OFF transient alpha, n = 4; ON sustained, n = 6.

(E) Smallest texture scale for which the response reached 85% of its maximum for individual cells in (D) (average ± SEM within each group of cells). This value was the smallest for OND RGCs: relative to ON sustained RGCs, *$p < 0.05$; to all other groups, **$p < 0.01$; one-tailed unpaired t test.

(change in lens shape) may be absent in the mouse [47], the pupillary near reflex, adjusting the depth of focus to the target distance [49–51], may well be present [52].

Future work identifying genetic markers of the OND RGC and tracing its projections in the brain will be needed in order to establish its role in reporting image focus or in other functions.

EXPERIMENTAL PROCEDURES

Electrophysiology experiments were performed on retinas from wild-type mice presented with visual stimuli as described previously [16, 22]. All animal procedures were approved by the Institutional Animal Care and Use Committee of the Center for Comparative Medicine at Northwestern University. Methodological details, including data and image analysis and modeling, can be found in the Supplemental Experimental Procedures.

SUPPLEMENTAL INFORMATION

Supplemental Information includes Supplemental Experimental Procedures and five figures and can be found with this article online at http://dx.doi.org/10.1016/j.cub.2016.12.033.

AUTHOR CONTRIBUTIONS

A.M. and G.W.S. designed research, performed research, analyzed data, and wrote the paper.

ACKNOWLEDGMENTS

This work was supported by a Research to Prevent Blindness Career Development Award (to G.W.S.), NIH/Director's Fund and National Eye Institute grant DP2EY026770 (to G.W.S.), Karl Kirchgessner Foundation Vision Research Award (to G.W.S.), and Knights Templar Eye Foundation career starter grant (to A.M.). We deeply thank Susan L. Wohlgenant for technical support, Fred M. Rieke, Jon Cafaro, William N. Grimes, Michael B. Manookin, and Petri Ala-Laurila for reviewing earlier versions of this manuscript and providing critical feedback, and G.W.S. laboratory members for helpful discussions.

Received: April 29, 2016
Revised: November 10, 2016
Accepted: December 14, 2016
Published: January 26, 2017

REFERENCES

1. Kuffler, S.W. (1953). Discharge patterns and functional organization of mammalian retina. J. Neurophysiol. *16*, 37–68.
2. Wässle, H. (2004). Parallel processing in the mammalian retina. Nat. Rev. Neurosci. *5*, 747–757.
3. Thoreson, W.B., and Mangel, S.C. (2012). Lateral interactions in the outer retina. Prog. Retin. Eye Res. *31*, 407–441.
4. Lukasiewicz, P.D. (2005). Synaptic mechanisms that shape visual signaling at the inner retina. Prog. Brain Res. *147*, 205–218.
5. Münch, T.A., da Silveira, R.A., Siegert, S., Viney, T.J., Awatramani, G.B., and Roska, B. (2009). Approach sensitivity in the retina processed by a multifunctional neural circuit. Nat. Neurosci. *12*, 1308–1316.
6. Hoggarth, A., McLaughlin, A.J., Ronellenfitch, K., Trenholm, S., Vasandani, R., Sethuramanujam, S., Schwab, D., Briggman, K.L., and Awatramani, G.B. (2015). Specific wiring of distinct amacrine cells in the directionally selective retinal circuit permits independent coding of direction and size. Neuron *86*, 276–291.
7. Zhang, Y., Kim, I.J., Sanes, J.R., and Meister, M. (2012). The most numerous ganglion cell type of the mouse retina is a selective feature detector. Proc. Natl. Acad. Sci. USA *109*, E2391–E2398.
8. Ölveczky, B.P., Baccus, S.A., and Meister, M. (2003). Segregation of object and background motion in the retina. Nature *423*, 401–408.
9. Dhande, O.S., Estevez, M.E., Quattrochi, L.E., El-Danaf, R.N., Nguyen, P.L., Berson, D.M., and Huberman, A.D. (2013). Genetic dissection of retinal inputs to brainstem nuclei controlling image stabilization. J. Neurosci. *33*, 17797–17813.
10. Gollisch, T., and Meister, M. (2010). Eye smarter than scientists believed: neural computations in circuits of the retina. Neuron *65*, 150–164.
11. Sanes, J.R., and Masland, R.H. (2015). The types of retinal ganglion cells: current status and implications for neuronal classification. Annu. Rev. Neurosci. *38*, 221–246.
12. Baden, T., Berens, P., Franke, K., Román Rosón, M., Bethge, M., and Euler, T. (2016). The functional diversity of retinal ganglion cells in the mouse. Nature *529*, 345–350.
13. Kim, T., Soto, F., and Kerschensteiner, D. (2015). An excitatory amacrine cell detects object motion and provides feature-selective input to ganglion cells in the mouse retina. eLife *4*, e08025.
14. Zhao, X., Stafford, B.K., Godin, A.L., King, W.M., and Wong, K.Y. (2014). Photoresponse diversity among the five types of intrinsically photosensitive retinal ganglion cells. J. Physiol. *592*, 1619–1636.
15. Dumitrescu, O.N., Pucci, F.G., Wong, K.Y., and Berson, D.M. (2009). Ectopic retinal ON bipolar cell synapses in the OFF inner plexiform layer: contacts with dopaminergic amacrine cells and melanopsin ganglion cells. J. Comp. Neurol. *517*, 226–244.
16. Nath, A., and Schwartz, G.W. (2016). Cardinal orientation selectivity is represented by two distinct ganglion cell types in mouse retina. J. Neurosci. *36*, 3208–3221.
17. Sümbül, U., Song, S., McCulloch, K., Becker, M., Lin, B., Sanes, J.R., Masland, R.H., and Seung, H.S. (2014). A genetic and computational approach to structurally classify neuronal types. Nat. Commun. *5*, 3512.
18. Völgyi, B., Chheda, S., and Bloomfield, S.A. (2009). Tracer coupling patterns of the ganglion cell subtypes in the mouse retina. J. Comp. Neurol. *512*, 664–687.
19. Sivyer, B., and Vaney, D.I. (2010). Dendritic morphology and tracer-coupling pattern of physiologically identified transient uniformity detector ganglion cells in rabbit retina. Vis. Neurosci. *27*, 159–170.
20. Tien, N.-W., Pearson, J.T., Heller, C.R., Demas, J., and Kerschensteiner, D. (2015). Genetically identified suppressed-by-contrast retinal ganglion cells reliably signal self-generated visual stimuli. J. Neurosci. *35*, 10815–10820.
21. Lee, S., Zhang, Y., Chen, M., and Zhou, Z.J. (2016). Segregated glycine-glutamate co-transmission from vGluT3 amacrine cells to contrast-suppressed and contrast-enhanced retinal circuits. Neuron *90*, 27–34.
22. Jacoby, J., Zhu, Y., DeVries, S.H., and Schwartz, G.W. (2015). An amacrine cell circuit for signaling steady illumination in the retina. Cell Rep. *13*, 2663–2670.
23. Helmstaedter, M., Briggman, K.L., Turaga, S.C., Jain, V., Seung, H.S., and Denk, W. (2013). Connectomic reconstruction of the inner plexiform layer in the mouse retina. Nature *500*, 168–174.
24. Masri, R.A., Percival, K.A., Koizumi, A., Martin, P.R., and Grünert, U. (2016). Connectivity between the OFF bipolar type DB3a and six types of ganglion cell in the marmoset retina. J. Comp. Neurol. *524*, 1839–1858.
25. Farrow, K., Teixeira, M., Szikra, T., Viney, T.J., Balint, K., Yonehara, K., and Roska, B. (2013). Ambient illumination toggles a neuronal circuit switch in the retina and visual perception at cone threshold. Neuron *78*, 325–338.
26. Gollisch, T., and Meister, M. (2008). Rapid neural coding in the retina with relative spike latencies. Science *319*, 1108–1111.
27. Koch, C., Poggio, T., and Torre, V. (1982). Retinal ganglion cells: a functional interpretation of dendritic morphology. Philos. Trans. R. Soc. Lond. B Biol. Sci. *298*, 227–263.
28. Masland, R.H. (2001). The fundamental plan of the retina. Nat. Neurosci. *4*, 877–886.

29. Freed, M.A., Smith, R.G., and Sterling, P. (1992). Computational model of the on-alpha ganglion cell receptive field based on bipolar cell circuitry. Proc. Natl. Acad. Sci. USA *89*, 236–240.

30. Berntson, A., and Taylor, W.R. (2000). Response characteristics and receptive field widths of on-bipolar cells in the mouse retina. J. Physiol. *524*, 879–889.

31. Schwartz, G.W., Okawa, H., Dunn, F.A., Morgan, J.L., Kerschensteiner, D., Wong, R.O., and Rieke, F. (2012). The spatial structure of a nonlinear receptive field. Nat. Neurosci. *15*, 1572–1580.

32. Hille, B. (2001). Ion Channels of Excitable Membranes, Third Edition (Sinauer Associates).

33. Sivyer, B., Van Wyk, M., Vaney, D.I., and Taylor, W.R. (2010). Synaptic inputs and timing underlying the velocity tuning of direction-selective ganglion cells in rabbit retina. J. Physiol. *588*, 3243–3253.

34. Venkataramani, S., Van Wyk, M., Buldyrev, I., Sivyer, B., Vaney, D.I., and Taylor, W.R. (2014). Distinct roles for inhibition in spatial and temporal tuning of local edge detectors in the rabbit retina. PLoS ONE *9*, e88560.

35. Manookin, M.B., Beaudoin, D.L., Ernst, Z.R., Flagel, L.J., and Demb, J.B. (2008). Disinhibition combines with excitation to extend the operating range of the OFF visual pathway in daylight. J. Neurosci. *28*, 4136–4150.

36. Eggers, E.D., and Lukasiewicz, P.D. (2010). Interneuron circuits tune inhibition in retinal bipolar cells. J. Neurophysiol. *103*, 25–37.

37. Eggers, E.D., and Lukasiewicz, P.D. (2011). Multiple pathways of inhibition shape bipolar cell responses in the retina. Vis. Neurosci. *28*, 95–108.

38. Zhang, C., and McCall, M.A. (2012). Receptor targets of amacrine cells. Vis. Neurosci. *29*, 11–29.

39. Gütig, R., Gollisch, T., Sompolinsky, H., and Meister, M. (2013). Computing complex visual features with retinal spike times. PLoS ONE *8*, e53063.

40. Bölinger, D., and Gollisch, T. (2012). Closed-loop measurements of iso-response stimuli reveal dynamic nonlinear stimulus integration in the retina. Neuron *73*, 333–346.

41. Shapley, R.M., and Victor, J.D. (1978). The effect of contrast on the transfer properties of cat retinal ganglion cells. J. Physiol. *285*, 275–298.

42. Berson, D.M., Dunn, F.A., and Takao, M. (2002). Phototransduction by retinal ganglion cells that set the circadian clock. Science *295*, 1070–1073.

43. Burge, J., and Geisler, W.S. (2011). Optimal defocus estimation in individual natural images. Proc. Natl. Acad. Sci. USA *108*, 16849–16854.

44. Umino, Y., Solessio, E., and Barlow, R.B. (2008). Speed, spatial, and temporal tuning of rod and cone vision in mouse. J. Neurosci. *28*, 189–198.

45. Pardue, M.T., Stone, R.A., and Iuvone, P.M. (2013). Investigating mechanisms of myopia in mice. Exp. Eye Res. *114*, 96–105.

46. Daw, N.W. (2014). Visual Development (Springer).

47. Schmucker, C., and Schaeffel, F. (2004). A paraxial schematic eye model for the growing C57BL/6 mouse. Vision Res. *44*, 1857–1867.

48. Chakraborty, R., Park, H.N., Hanif, A.M., Sidhu, C.S., Iuvone, P.M., and Pardue, M.T. (2015). ON pathway mutations increase susceptibility to form-deprivation myopia. Exp. Eye Res. *137*, 79–83.

49. Kaufman, P.L., Alm, A., and Adler, F.H. (2003). Adler's Physiology of the Eye: Clinical Application (Mosby).

50. Beatty, J., and Lucero-Wagoner, B. (2000). The pupillary system. In Handbook of Psychophysiology, Second Edition, J.T. Cacioppo, L.G. Tassinary, and G.G. Berntson, eds. (Cambridge University Press), pp. 142–162.

51. Bando, T., Takagi, M., Toda, H., and Yoshizawa, T. (1992). Functional roles of the lateral suprasylvian cortex in ocular near response in the cat. Neurosci. Res. *15*, 162–178.

52. Pinto, L.H., and Enroth-Cugell, C. (2000). Tests of the mouse visual system. Mamm. Genome *11*, 531–536.